NANO LETTERS

pubs.acs.org/NanoLett Letter

Graphene Whisperitronics: Transducing Whispering Gallery Modes into Electronic Transport

Boris Brun,* Viet-Hung Nguyen, Nicolas Moreau, Sowmya Somanchi, Kenji Watanabe, Takashi Taniguchi, Jean-Christophe Charlier, Christoph Stampfer, and Benoit Hackens*

Cite This: *Nano Lett.* 2022, 22, 128−134 Read Online

ABSTRACT: When confined in circular cavities, graphene relativistic charge carriers occupy whispering gallery modes (WGMs) in analogy to classical acoustic and optical fields. The rich geometrical patterns of the WGMs decorating the local density of states offer promising perspectives to devise new disruptive quantum devices. However, exploiting these highly sensitive resonances requires the transduction of the WGMs to the outside world through source and drain electrodes, a yet unreported configuration. Here, we create a circular p−n island in a graphene device using a polarized scanning gate microscope tip and probe the resulting WGM signatures in in-plane electronic transport through the p−n island. Combining tight-binding simulations and the exact solution of the Dirac equation, we assign the measured device conductance features to WGMs and demonstrate mode selectivity by displacing the p−n island with respect to a constriction. This work therefore constitutes a proof of concept for graphene whisperitronic devices.

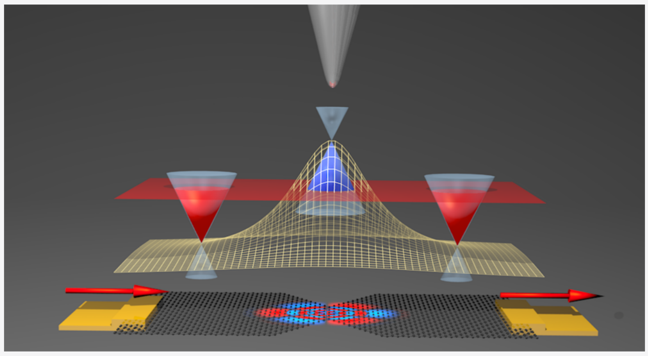

KEYWORDS: *Graphene, scanning gate microscopy, quantum transport, whispering gallery modes*

■ INTRODUCTION

Whispering gallery modes (WGMs) denote the guided waves circulating along a concave surface, the seminal example of this phenomenon occurring in the whispering galleries of St. Paul's Cathedral with acoustic waves. This originally macroscopic-scale phenomenon found rich applications in nanotechnology with the ability to design resonating galleries, e.g., for electromagnetic waves, with nanometer-scale precision.[1,2] Taking advantage of the high quality factor and the reduced size of optical and mechanical whispering nanoresonators, a new class of ultrasensitive detectors has recently been developed, stretching the limits of physical and biological quantity detection down to a single molecule or virus.[3,4] In the nanoelectronic world, WGMs have proven successful to achieve distant coupling between GaAs quantum dots.[5] Recently, electronic WGMs have been reported in graphene,[6] offering promising perspectives to develop a new class of devices, taking advantage of the sensitivity of these geometrical resonances combined with the high technological integrability of graphene.

Graphene charge carriers behave as relativistic massless particles,[7] therefore sharing part of their fundamental properties with photons. Consequently, graphene has long been proposed as an ideal platform to realize electron-optics experiments, in which p−n junctions play the role of lenses, prisms, or fibers and are used to guide, refract, and transmit electrons and holes, taking advantage of Klein tunneling.[8−14] As a seminal example of Dirac fermion optics, it has long been proposed[15] and observed[16] that Fabry−Pérot (FP) interferences can arise between two facing p−n junctions, acting as semireflecting mirrors. When considering a circular p−n junction, FP interference patterns then correspond to concentric rings, indeed visible in simulated wave functions.[6] But FP interferences are only a subclass of a larger set of WGMs: at a larger angular momentum m, a manifold of patterns mixing radial and concentric symmetries emerge due to circular geometric symmetry, enriching the existing palette of Dirac fermion optics.

Up to now, evidencing graphene p−n island WGMs has relied on the use of a scanning tunneling microscope (STM),[6,17] probing the local density of states (LDOS) through tunneling between the island and a metallic tip. However, the practical integration of WGM-supporting p−n islands in future electronic devices will require to incorporate them in electron-optics setups and combine them with other

Received: September 5, 2021
Revised: December 2, 2021
Published: December 13, 2021

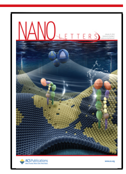

https://doi.org/10.1021/acs.nanolett.1c03451
Nano Lett. 2022, 22, 128−134

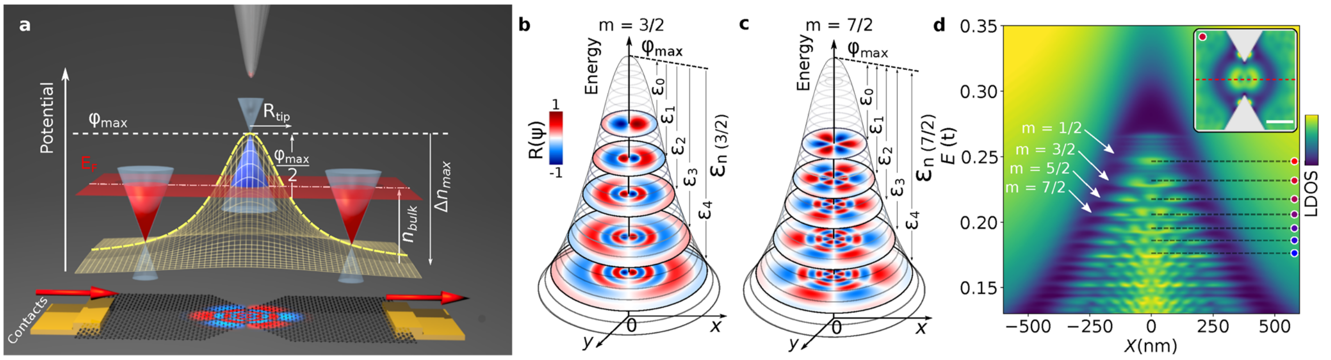

Figure 1. Whisperitronics, transducing graphene whispering gallery modes to external contacts: (a) Scheme of the electrostatic potential landscape: a biased AFM tip induces a Lorentzian potential whose maximum is φ_{max} and half-width at half-maximum is R_{tip}, centered on a graphene constriction doped at a Fermi energy E_F. Electronic transport is measured through the WGMs induced in the p−n island; the p region is below the tip. One WGM wave function is plotted at the center with red and blue colors. (b) Real part of the wave function $\mathcal{R}(\psi_m(x, y))$ corresponding to the angular momentum $m = 3/2$, at different resonant energies, calculated by solving the radial Dirac equation in the presence of a Lorentzian potential, in an isotropic plane, without constriction. (c) $\mathcal{R}(\psi_m(x, y))$ for $m = 7/2$, showing higher angular symmetry patterns. (d) LDOS in a p−n island, placed at the center of a 240 nm wide graphene constriction, as a function of energy E in units of the hopping parameter t and the x position along the red dashed line in the inset. Inset: LDOS map for the third resonant mode. Scale bar: 200 nm.

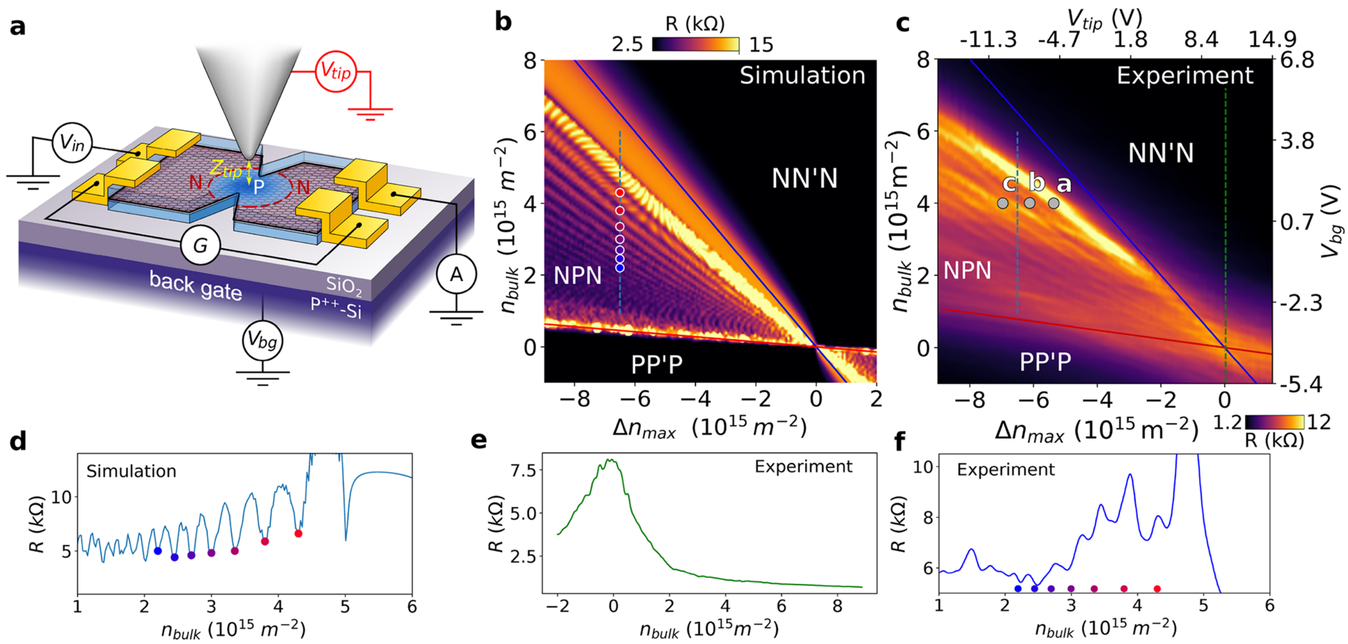

Figure 2. Transport through WGMs in a constriction. (a) Scheme of the experiment: a polarized AFM tip is placed above a constriction defined in encapsulated graphene. The tip potential is discussed in section 5 of the Supporting Information. (b) Calculated resistance as a function of the sheet carrier density n_{bulk} and the maximum density change Δn_{max}, exhibiting oscillations in the N−P−N configuration. The value of $\Delta n_{max} = -6.5 \times 10^{15}$ m^{-2} used in Figures 1d and 2d is indicated by a blue dashed line as well as the six first resistance minima in this configuration that are labeled by colored dots (red to blue), reported in Figures 1d and 2d for comparison. N′ and P′ denote the carrier nature in the tip-pertubed region when it is similar to the sheet carrier type. The blue line indicates the N−N′−N/N−P−N limit $n_{bulk} = -\Delta n_{max}$. Note that it does not coincide with the resistance maximum. (c) Calculated resistance versus n_{bulk}, for $\Delta n_{max} = -6.5 \times 10^{15}$ m^{-2}. (d) Resistance as a function of V_{tip} and V_{bg}, recorded by placing the tip above the constriction at a distance $Z_{tip} = 90$ nm from the graphene plane. Couples of V_{tip} and V_{bg} values for which the SGM images in Figure 3a−c are recorded as indicated by dots. (e) Constriction resistance as a function of n_{bulk}, for a neutral tip ($\Delta n_{max} = 0$, green dashed line in c). (f) Constriction resistance as a function of n_{bulk}, for $V_{tip} = -11$ V ($\Delta n_{max} = -6.5 \times 10^{15}$ m^{-2}) and $Z_{tip} = 90$ nm, corresponding to blue dashed line in c. Colored dots correspond to minima in the simulated data (in Figure 2d).

Dirac fermion optics tools.[12−14] This transduction of the WGM devices to the outside world requires driving current between in-plane electrical contacts, a configuration in which WGMs have not been demonstrated in graphene to date.

Here, we demonstrate the detection and manipulation of WGMs in in-plane transport *through* a circular encapsulated graphene p−n junction, the essential ingredient to realize a new class of whisperitronics devices. The p−n junction is created using the polarized tip of a scanning gate microscope (SGM),[18,19] which can be moved in the vicinity of a constriction (Figure 1a). This demonstrates a surprising robustness of WGMs with respect to geometrical pinching of the circular island inside the constriction. Ultimately, the WGM selectivity is revealed by displacing laterally the p−n island with respect to the constriction, offering a very high degree of tunability. Consequently, our work paves the way

https://doi.org/10.1021/acs.nanolett.1c03451
Nano Lett. 2022, 22, 128−134

toward controllable whisperitronics, merging these freshly revealed WGMs[6] with the existing graphene electron-optics palette.

■ RESULTS

Charge carriers in a graphene p−n island occupy a rich set of states,[6,20−22] labeled by different angular momenta m, each of them exhibiting several resonant energies as exemplified in Figure 1b,c. To sense these different WGMs using in-plane electronic transport, the easiest way is to connect the resonator to two separate graphene regions by pinching the p−n island in a narrow channel, e.g., an etched constriction, as schemed in Figures 1a and 2a. Surprisingly, the WGMs are really robust and survive when placing the p−n island in such a constriction. This remarkable fact is demonstrated in Figure 1d, where we plot the LDOS profile along the transport axis in a circular p−n junction placed at the center of a 240 nm wide constriction. Despite the constriction, the pattern is strikingly similar to the unperturbed p−n island case (see section 3 of the Supporting Information). Noteworthily, the resonant states yield LDOS patterns that extend in the low-density region (indicated by white arrows Figure 1d), as shown experimentally in STM in refs 17 and 23 and supported by recent theoretical explorations.[24] The assignment of different m values to these LDOS extensions is made possible by explicit comparison of the tight-binding simulations shown in Figure 1d (obtained using the Kwant code[25] with proper scaling[26] as well as a homemade recursive green function code[27]), with the exact solution of the Dirac equation[28] (see sections 2−3 of the Supporting Information).

The total resistance of the WGM resonator exhibits strong oscillations versus carrier density, as shown by Figure 2b,d. Remarkably, the resistance minima correspond to the extended WGMs, as indicated by the color dots showing the resonant energies of WGMs in Figure 1d, translated in carrier density and reported on the calculated resistance plots of Figure 2b,d. This is surprising, since WGMs arise due to internal reflections of the Dirac fermions on the border of the resonator. On the other hand, they yield a nonzero LDOS in the low-density region at the edge, which favors a coupling with the Dirac continuum of states outside the resonator. These competing effects counterintuitively result in a low total resistance. Finally, we show in Figure 2b the evolution of the resistance oscillations with n_{bulk} and Δn_{max}, which correspond to the evolution of the different WGMs with energy and potential strength. Noticeably, these oscillations are not equally spaced in n_{bulk}, and their spacing increases as Δn_{max} is made more negative. The location of minima also strongly depends on the geometry of the junction, as discussed in section 6 of the Supporting Information. This configuration of a circular Dirac fermion resonator embedded in a constriction is therefore expected to exhibit strong signatures of WGMs in electrical transport.

We now provide an experimental demonstration of this theoretical prediction, by generating a tunable p−n junction in a graphene device[19] using the polarized metallic tip of an atomic force microscope.[18] Scanning gate microscopy (SGM) consists of scanning a polarized tip in the vicinity of a mesoscopic device while recording its conductance. It was initially developed to study mesoscopic phenomena in III−V semiconductor heterostructures,[29,30] in which an insulating layer prevents tunneling from an STM tip to the surface, and has been successfully been extended to the study of transport in graphene devices.[31−33] The sample (see methods), consists of an h-BN-encapsulated monolayer graphene flake, in which a 250 nm wide constriction is defined by etching,[34] consistent with the geometry defined in the simulation. We first place the tip 90 nm above the constriction center, as sketched in Figure 2a, and record the device resistance R while varying the tip and backgate voltages V_{tip} and V_{bg}, the experimental knobs linearly related to Δn_{max} and n_{bulk} through the relations $\Delta n_{max} = C_{tip}(V_{tip} - V^0_{tip})$ and $n_{bulk} = C_{bg}(V_{bg} - V^0_{bg})$, where C_{tip} is the tip−graphene capacitance, C_{bg} is the back-gate capacitance, and V^0_{tip} and V^0_{bg} are the charge neutrality points when sweeping the tip and back-gate voltages, respectively. Details about the determination of the capacitances and neutrality voltages are provided in the Supporting Information. The result, measured at low temperature (4.2 K), is shown in Figure 2c, where different regions can be identified (NN′N, NPN, or PP′P), depending on the type of charge carriers below the tip and in the regions away from the constriction. When the tip voltage compensates its work function, i.e., $\Delta n_{max} = 0$, one recovers an unpertubed behavior of the sample, and the resistance shows a single maximum at the Dirac point, as shown in Figure 2e. Conversely, quasiperiodic oscillations are visible in the n−p−n configuration, similar to the corresponding simulation of Figure 2b. This corresponds to a bulk occupied by electrons and holes in the tip-perturbed region. For comparison, we plot in Figure 2f the resistance as a function of n_{bulk} for a tip voltage of −11 V, corresponding to $\Delta n_{max} = -6.5 \times 10^{15}$ m^{-2}, similar to the calculation presented in Figure 2d. The qualitative agreement in the evolution of the oscillations in Figure 2d,f in the range between 2×10^{15} and 5×10^{15} m^{-2} and, in particular, in the positions of the seven minima marked by colored dots in Figure 2d, represent a first hint that the experimental resistance oscillations correspond to the internal WGMs of the p−n island.

However, the patterns of Figure 2b,c are reminiscent of FP oscillations observed in straight gate-defined n−p−n junctions.[16,35] In a recent work,[36] we showed that when the tip is centered above the constriction, these tip-induced oscillations exhibit similarities with FP oscillations. In particular, their contrast can be controlled by the potential smoothness that governs the quasiconfinement of Dirac fermions. Indeed, FP oscillations share a common ground with WGM oscillations, both arising due to the coherent superposition of waves in a confined geometry. However, as indicated above, FP are actually a subclass of WGMs in circular or elliptic cavities, corresponding to the fundamental angular momentum m. The main question at this point is therefore whether signatures of higher-order symmetry WGMs can be clearly evidenced and controlled when charge carriers are transmitted through the circular cavity, making new quantum whisperitronic applications possible.

To reveal the wealth of oscillations arising from internal resonances of the tip-induced p−n island, one needs to off-center the tip with respect to the constriction. Intuitively, gradually overlapping the circular cavity with the etched triangle-shaped edges of the constriction will strongly alter high-angular-momentum radial resonances, as it will break circular symmetry. We first scan the polarized tip around the constriction and map out resistance as a function of tip position for different V_{tip} and V_{bg}, yielding the SGM maps shown in Figure 3a−c (top panels). We showed in ref 19 that the resistance maps obtained in this type of experiment reflect the average Dirac fermion flow through the p−n island. Here,

https://doi.org/10.1021/acs.nanolett.1c03451
Nano Lett. 2022, 22, 128−134

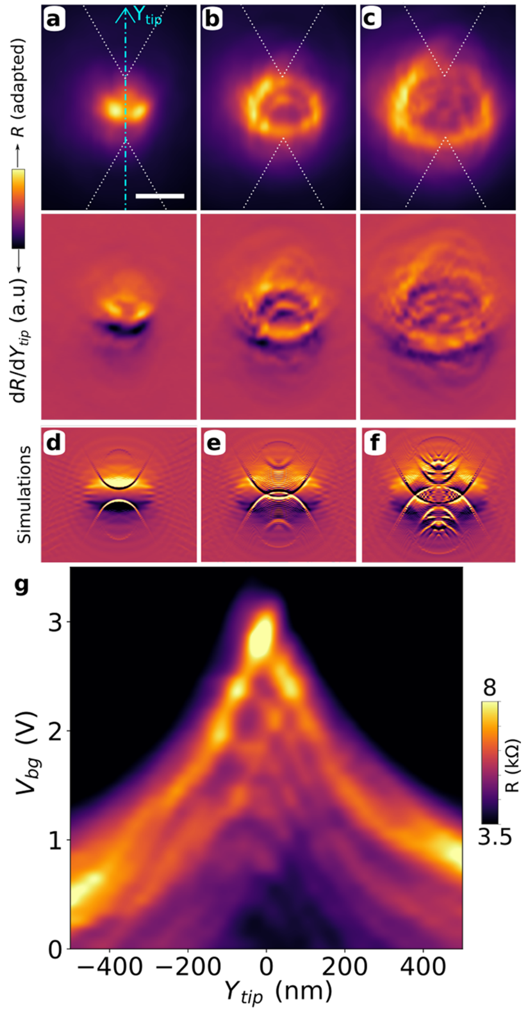

Figure 3. Experiment: Scanning gate microscopy images and spectroscopy. (a−c) Up: SGM images, i.e., device resistance as a function of X_{tip} and Y_{tip}, for V_{bg} = +1.5 V, Z_{tip} = 90 nm, and V_{tip} = −6 V (a), −8 V (b), and −10 V (c). Scale bar: 200 nm. The resistance color scale has been adapted for each image. Down: derivative of the same SGM images versus Y_{tip} (vertical direction). (d−f) Simulated differentiated SGM maps, for three different tip-induced density changes corresponding to the experimental conditions of a−c, respectively. (g) Measured resistance as a function of V_{bg} and tip position along the blue dash-dotted line in Figure 3a, for a tip voltage V_{tip} = −14 V and a tip-to-graphene distance Z_{tip} = 110 nm.

we go one step further with higher-resolution SGM maps and spectroscopies, showing that displacing the p−n island with respect to the constriction allows its internal LDOS resonances to be probed. In the bottom panels of Figure 3a−c, we plot the derivative of the resistance versus the *y*-direction (transverse to transport axis) for each of the top panels' maps. The differentiated maps better highlight oscillations discussed in the remaining part of the paper. These maps indeed exhibit arcs centered on the constriction apexes, which are limited to the constriction area. Such arcs are fundamentally different from the usually observed concentric circles, ubiquitous in SGM of quantum dots[37−39] or disordered systems.[32,40,41] The latter circles correspond to Coulomb blockade peaks forming when the confined resonant modes associated with local cavities induced, e.g., by disorder, are raised locally to the Fermi level by the gating action of the tip. Contrary to Coulomb-blockade-related circles, the arcs visible in Figure 3b,c can be reproduced by single-particle tight-binding simulations, as shown in Figure 3d−f where we present the simulated SGM maps differentiated versus Y_{tip}. This therefore rules out a possible Coulombic origin.

To clarify the origin of SGM arcs, we scan the tip along a line transverse to transport axis (blue dash-dotted line in Figure 3a) while varying continuously V_{bg} and plot the resulting resistance map in Figure 3g. The overall envelope delineating the high-resistance region in the lower part of Figure 3g (corresponding to n−p−n junction) reflects the tip-induced potential and can be fitted to evaluate it accurately (see refs 19 and 36 and section 6 of the Supporting Information). Within this high-resistance region, local resistance maxima undergo the same Lorentzian evolution, with a lateral offset with respect to the envelope, and lead to higher-resistance spots at their crossing points. These successive maxima correspond to the interference observed in Figure 2f and the SGM arcs in Figure 3b,c. Figure 3g reveals that these modes are brought to lower bulk energy (i.e., higher energy in the island) when displacing laterally the tip with respect to the constriction center, i.e., when the p−n island overlaps with the constriction side.

To understand this observation, we perform additional tight-binding simulations and show the evolution of the LDOS in the p−n island when displacing it along the axis transverse to the constriction axis in Figure 4a,b, for two different energies. From these maps, the role of the constriction on the resonator WGMs is clarified: bringing the tip-induced p−n junction

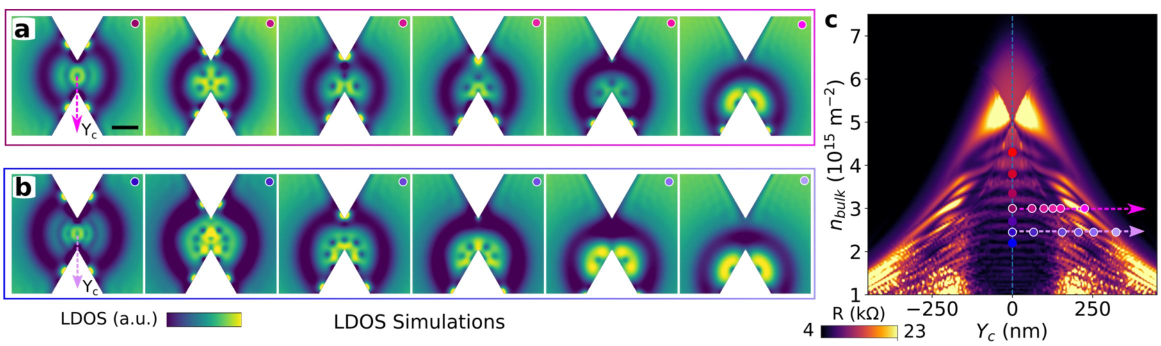

Figure 4. Selective transmission of WGMs by lateral displacement: (a) LDOS calculated for the same tip potential as in Figure 2, for different tip positions along the *y*-axis as marked in (c). Scale bar: 200 nm. (b) Same data calculated for a lower bulk energy (i.e., higher energy—hence smaller Fermi wavelength—in the resonator). Corresponding energies and tip positions are indicated by colored dots in c. (c) Calculated resistance as a function of energy and lateral p−n island displacement Y_c, for the same potential as in Figures 1d, 2d, and 4a,b.

above the etched region reduces the available area for the carriers in the p−n island and consequently promotes lower angular momentum modes in the resonator. Indeed, depending on the starting eigenmode, a well-defined number of local LDOS minima are clearly visible as soon as the p−n island is off-centered by a few tens of nanometers, as visible in the second panels of Figure 4a,b. This number of "holes" is then reduced one by one as the p−n island is brought away from the constriction center (see Supplementary Movies SM 1−2). This illustrates that WGMs are morphology-dependent resonances that can be modified by changing the resonator geometry.

Finally, we present in Figure 4c the calculated resistance as a function of density and tip position along the y-axis Y_c. Though richer details are present compared to the experimental data of Figure 3g, the average evolution of the calculated resistance is consistent with the measurement, indicating that the different resonant modes energies are brought to lower bulk density (hence, higher hole density in the p−n island) when the tip-induced potential overlaps with the etched region.

DISCUSSION

Our results demonstrate two different ways to selectively address the different electrical WGMs of the Dirac Fermion resonator:

(i) Playing independently on V_{tip} and V_{bg} allows different WGMs to be clearly selected, with strong fingerprints in the current through the p−n island. This contrasts with STM experiments, where the tip bias not only changes the resonator shape but also affects the injection energy of charge carriers, leading to a spurious replication of the WGMs at the tip bias energy.[6] Here, the injection energy can be tuned completely independently, since the tip and the graphene plane are only capacitively connected so that the intrinsic behavior of WGMs can be more readily accessed.

(ii) Displacing the p−n island laterally with respect to the constriction also allows the different WGMs to be selectively addressed. This is a promising configuration, since it is analogous to the configuration used in high-quality factor optomechanical resonators, where the readout line is side-coupled to the WGMs of the resonator and allows for ultrafast and sensitive readout of the resonator state.[42]

We would like to emphasize that in the studied geometry, both radial ("Fabry−Pérot" like) and higher-angular-momentum WGM resonances contribute to transport. Engineering further the p−n junction potential and increasing the quality and geometry of the constriction may allow in the future the different modes' contributions to transport to be accurately selected. Additional possibilities for coupling WGMs and a transport channel, as well as for addressing individual WGMs, can also be envisioned. For example, in analogy with the geometry of some optical WGM devices, we anticipate that lateral tunnel coupling of a propagating one-dimensional graphene channel with a circular resonating cavity would provide an even more sensitive and tunable platform to probe individual WGMs. It would indeed combine a less invasive approach with the extreme tunability of coupling offered by the tunnel barrier. Finally, the high quality factor required to improve the sensitivity of such devices can readily be engineered by tuning the potential smoothness, as reported in ref 36. Opening the way toward such perspectives, this work bridges the recently discovered WGMs of graphene p−n islands with the field of Dirac fermion optics, heralding the advent of relativistic whisperitronics, a promising field for the engineering of disruptive quantum devices.

ASSOCIATED CONTENT

Supporting Information

The Supporting Information is available free of charge at https://pubs.acs.org/doi/10.1021/acs.nanolett.1c03451.

Figures S1 to S6 and a text detailing sample and measurement methods, individual contributions of the WGMs to the total LDOS, labeling the WGMs in transport, scaling of the tight-binding model, tip-induced potential, simulation of SGM images, and effect of the npn junction shape on WGM resonances (PDF)

Evolution of LDOS for the sixth resonant mode when displacing the tip perpendicular to transport axis (MOV)

Evolution of LDOS for the fourth resonant mode when displacing the tip perpendicular to transport axis (MOV)

AUTHOR INFORMATION

Corresponding Authors

Boris Brun − *IMCN/NAPS & MODL, Université catholique de Louvain (UCLouvain), B-1348 Louvain-la-Neuve, Belgium;* orcid.org/0000-0001-7403-2484; Email: boris.brun@uclouvain.be

Benoit Hackens − *IMCN/NAPS & MODL, Université catholique de Louvain (UCLouvain), B-1348 Louvain-la-Neuve, Belgium;* orcid.org/0000-0001-6121-5126; Email: benoit.hackens@uclouvain.be

Authors

Viet-Hung Nguyen − *IMCN/NAPS & MODL, Université catholique de Louvain (UCLouvain), B-1348 Louvain-la-Neuve, Belgium;* orcid.org/0000-0001-6729-3520

Nicolas Moreau − *IMCN/NAPS & MODL, Université catholique de Louvain (UCLouvain), B-1348 Louvain-la-Neuve, Belgium*

Sowmya Somanchi − *JARA-FIT and 2nd Institute of Physics, RWTH Aachen University, 52062 Aachen, Germany; Peter Grünberg Institute (PGI-9), Forschungszentrum Jülich, 52425 Jülich, Germany*

Kenji Watanabe − *Research Center for Functional Materials, National Institute for Materials Science, Tsukuba 305-0044, Japan;* orcid.org/0000-0003-3701-8119

Takashi Taniguchi − *International Center for Materials Nanoarchitectonics, National Institute for Materials Science, Tsukuba 305-0044, Japan;* orcid.org/0000-0002-1467-3105

Jean-Christophe Charlier − *IMCN/NAPS & MODL, Université catholique de Louvain (UCLouvain), B-1348 Louvain-la-Neuve, Belgium*

Christoph Stampfer − *JARA-FIT and 2nd Institute of Physics, RWTH Aachen University, 52062 Aachen, Germany; Peter Grünberg Institute (PGI-9), Forschungszentrum Jülich, 52425 Jülich, Germany;* orcid.org/0000-0002-4958-7362

Complete contact information is available at: https://pubs.acs.org/10.1021/acs.nanolett.1c03451

Notes

The authors declare no competing financial interest.

■ ACKNOWLEDGMENTS

We thank Prof. J.A. Stroscio for enthusiastic support and valuable input. B.B. thanks C. Groth for valuable help regarding Kwant simulations. Computational resources have been provided by the Consortium des Équipements de Calcul Intensif (CÉCI), funded by the Fonds de la Recherche Scientifique de Belgique (F.R.S.-FNRS) under Grant No. 2.502 0.11 and by the Walloon Region. The present research was funded by the Fédération Wallonie-Bruxelles through the ARC Grants No. 16/21-077 and No. 21/26-116 and from the European Union's Horizon 2020 Research and Innovation program (Core 3 − No. 881603). B.B. (research assistant), N.M. (FRIA fellowship), B.H. (research associate and PDR No. T.0105.21), V.-H.N. and J.-C.C. (PDR No. T.1077.15 and ERA-Net No. R.50.07.18.F) acknowledge financial support from the F.R.S.-FNRS of Belgium. Support by the Helmholtz Nanoelectronic Facility (HNF), the EU ITN SPINOGRAPH, and the DFG (SPP-1459) is gratefully acknowledged. This work was also supported by the FLAG-ERA grant TATTOOS, by the Deutsche Forschungsgemeinschaft (DFG, German Research Foundation) - 437 214 324. K.W. and T.T. acknowledge support from the Elemental Strategy Initiative conducted by the MEXT, Japan, Grant Number JPMXP0112101001, JSPS KAKENHI Grant Numbers JP20H00354 and the CREST(JPMJCR15F3), JST.

■ REFERENCES

(1) Vahala, K. J. Optical microcavities. *Nature* **2003**, *424*, 839−846.

(2) Foreman, M. R.; Swaim, J. D.; Vollmer, F. Whispering gallery mode sensors. *Adv. Opt. Photonics* **2015**, *7*, 168−240.

(3) Vollmer, F.; Arnold, S. Whispering-gallery-mode biosensing: label-free detection down to single molecules. *Nat. Methods* **2008**, *5*, 591−596.

(4) He, L.; Özdemir, S. K.; Zhu, J.; Kim, W.; Yang, L. Detecting single viruses and nanoparticles using whispering gallery microlasers. *Nat. Nanotechnol.* **2011**, *6*, 428−432.

(5) Nicolí, G.; Ferguson, M. S.; Rössler, C.; Wolfertz, A.; Blatter, G.; Ihn, T.; Ensslin, K.; Reichl, C.; Wegscheider, W.; Zilberberg, O. Cavity-Mediated Coherent Coupling between Distant Quantum Dots. *Phys. Rev. Lett.* **2018**, *120*, 236801.

(6) Zhao, Y.; Wyrick, J.; Natterer, F. D.; Rodriguez-Nieva, J. F.; Lewandowski, C.; Watanabe, K.; Taniguchi, T.; Levitov, L. S.; Zhitenev, N. B.; Stroscio, J. A. Creating and probing electron whispering-gallery modes in graphene. *Science* **2015**, *348*, 672−675.

(7) Novoselov, K. S.; Geim, A. K.; Morozov, S. V.; Jiang, D.; Katsnelson, M. I.; Grigorieva, I. V.; Dubonos, S. V.; Firsov, A. A. Two-dimensional gas of massless Dirac fermions in graphene. *Nature* **2005**, *438*, 197.

(8) Klein, O. Die Reflexion von Elektronen an einem Potential-sprung nach der relativistischen Dynamik von Dirac. *Eur. Phys. J. A* **1929**, *53*, 157−165.

(9) Cheianov, V. V.; Fal'ko, V.; Altshuler, B. L. The Focusing of Electron Flow and a Veselago Lens in Graphene p-n Junctions. *Science* **2007**, *315*, 1252−1255.

(10) Williams, J. R.; Low, T.; Lundstrom, M. S.; Marcus, C. M. Gate-controlled guiding of electrons in graphene. *Nat. Nanotechnol.* **2011**, *6*, 222.

(11) Rickhaus, P.; Liu, M.-H.; Makk, P.; Maurand, R.; Hess, S.; Zihlmann, S.; Weiss, M.; Richter, K.; Schönenberger, C. Guiding of Electrons in a Few-Mode Ballistic Graphene Channel. *Nano Lett.* **2015**, *15*, 5819−5825.

(12) Liu, M.-H.; Gorini, C.; Richter, K. Creating and Steering Highly Directional Electron Beams in Graphene. *Phys. Rev. Lett.* **2017**, *118*, 066801.

(13) Barnard, A. W.; Hughes, A.; Sharpe, A. L.; Watanabe, K.; Taniguchi, T.; Goldhaber-Gordon, D. Absorptive pinhole collimators for ballistic Dirac fermions in graphene. *Nat. Commun.* **2017**, *8*, 15418.

(14) Bøggild, P.; Caridad, J. M.; Stampfer, C.; Calogero, G.; Papior, N. R.; Brandbyge, M. A two-dimensional Dirac fermion microscope. *Nat. Commun.* **2017**, *8*, 15783.

(15) Shytov, A. V.; Rudner, M. S.; Levitov, L. S. Klein Backscattering and Fabry-Pérot Interference in Graphene Heterojunctions. *Phys. Rev. Lett.* **2008**, *101*, 156804.

(16) Young, A. F.; Kim, P. Quantum interference and Klein tunnelling in graphene heterojunctions. *Nat. Phys.* **2009**, *5*, 222.

(17) Ghahari, F.; Walkup, D.; Gutiérrez, C.; Rodriguez-Nieva, J. F.; Zhao, Y.; Wyrick, J.; Natterer, F. D.; Cullen, W. G.; Watanabe, K.; Taniguchi, T.; Levitov, L. S.; Zhitenev, N. B.; Stroscio, J. A. An on/off Berry phase switch in circular graphene resonators. *Science* **2017**, *356*, 845.

(18) Eriksson, M. A.; Beck, R. G.; Topinka, M.; Katine, J. A.; Westervelt, R. M.; Campman, K. L.; Gossard, A. C. Cryogenic scanning probe characterization of semiconductor nanostructures. *Appl. Phys. Lett.* **1996**, *69*, 671−673.

(19) Brun, B.; Moreau, N.; Somanchi, S.; Nguyen, V.-H.; Watanabe, K.; Taniguchi, T.; Charlier, J.-C.; Stampfer, C.; Hackens, B. Imaging Dirac fermions flow through a circular Veselago lens. *Phys. Rev. B: Condens. Matter Mater. Phys.* **2019**, *100*, 041401.

(20) Gutiérrez, C.; Brown, L.; Kim, C.-J.; Park, J.; Pasupathy, A. N. Klein tunnelling and electron trapping in nanometre-scale graphene quantum dots. *Nat. Phys.* **2016**, *12*, 1069.

(21) Lee, J.; Wong, D.; Velasco, J., Jr; Rodriguez-Nieva, J. F.; Kahn, S.; Tsai, H.-Z.; Taniguchi, T.; Watanabe, K.; Zettl, A.; Wang, F.; Levitov, L. S.; Crommie, M. F. Imaging electrostatically confined Dirac fermions in graphene quantum dots. *Nat. Phys.* **2016**, *12*, 1032.

(22) Jiang, Y.; Mao, J.; Moldovan, D.; Masir, M. R.; Li, G.; Watanabe, K.; Taniguchi, T.; Peeters, F. M.; Andrei, E. Y. Tuning a circular p−n junction in graphene from quantum confinement to optical guiding. *Nat. Nanotechnol.* **2017**, *12*, 1045.

(23) Gutiérrez, C.; Walkup, D.; Ghahari, F.; Lewandowski, C.; Rodriguez-Nieva, J. F.; Watanabe, K.; Taniguchi, T.; Levitov, L. S.; Zhitenev, N. B.; Stroscio, J. A. Interaction-driven quantum Hall wedding cake-like structures in graphene quantum dots. *Science* **2018**, *361*, 789.

(24) Le, T. L.; Nguyen, V. L. Quantitative study of electronic whispering gallery modes in electrostatic-potential induced circular graphene junctions. *J. Phys.: Condens. Matter* **2020**, *32*, 255502.

(25) Groth, C. W.; Wimmer, M.; Akhmerov, A. R.; Waintal, X. Kwant: a software package for quantum transport. *New J. Phys.* **2014**, *16*, 063065.

(26) Liu, M.-H.; Rickhaus, P.; Makk, P.; Tóvári, E.; Maurand, R.; Tkatschenko, F.; Weiss, M.; Schönenberger, C.; Richter, K. Scalable Tight-Binding Model for Graphene. *Phys. Rev. Lett.* **2015**, *114*, 036601.

(27) Hung Nguyen, V.; Bournel, A.; Dollfus, P. The conduction gap in double gate bilayer graphene structures. *J. Phys.: Condens. Matter* **2010**, *22*, 115304.

(28) Nguyen, V. H.; Charlier, J.-C. Klein tunneling and electron optics in Dirac-Weyl fermion systems with tilted energy dispersion. *Phys. Rev. B: Condens. Matter Mater. Phys.* **2018**, *97*, 235113.

(29) Topinka, M. A.; LeRoy, B. J.; Shaw, S. E. J.; Heller, E. J.; Westervelt, R. M.; Maranowski, K. D.; Gossard, A. C. Imaging Coherent Electron Flow from a Quantum Point Contact. *Science* **2000**, *289*, 2323−2326.

(30) Topinka, M. A.; LeRoy, B. J.; Westervelt, R. M.; Shaw, S. E. J.; Fleischmann, R.; Heller, E. J.; Maranowski, K. D.; Gossard, A. C. Coherent branched flow in a two-dimensional electron gas. *Nature* **2001**, *410*, 183−186.

(31) Connolly, M. R.; Chiu, K. L.; Lombardo, A.; Fasoli, A.; Ferrari, A. C.; Anderson, D.; Jones, G. A. C.; Smith, C. G. Tilted potential induced coupling of localized states in a graphene nanoconstriction. *Phys. Rev. B: Condens. Matter Mater. Phys.* **2011**, *83*, 115441.

https://doi.org/10.1021/acs.nanolett.1c03451
Nano Lett. 2022, 22, 128−134

(32) Pascher, N.; Bischoff, D.; Ihn, T.; Ensslin, K. Scanning gate microscopy on a graphene nanoribbon. *Appl. Phys. Lett.* **2012**, *101*, 063101.

(33) Garcia, A. G. F.; König, M.; Goldhaber-Gordon, D.; Todd, K. Scanning gate microscopy of localized states in wide graphene constrictions. *Phys. Rev. B: Condens. Matter Mater. Phys.* **2013**, *87*, 085446.

(34) Terrés, B.; Chizhova, L. A.; Libisch, F.; Peiro, J.; Jörger, D.; Engels, S.; Girschik, A.; Watanabe, K.; Taniguchi, T.; Rotkin, S. V.; Burgdörfer, J.; Stampfer, C. Size quantization of Dirac fermions in graphene constrictions. *Nat. Commun.* **2016**, *7*, 11528.

(35) Rickhaus, P.; Maurand, R.; Liu, M.-H.; Weiss, M.; Richter, K.; Schönenberger, C. Ballistic interferences in suspended graphene. *Nat. Commun.* **2013**, *4*, 2342.

(36) Brun, B.; Moreau, N.; Somanchi, S.; Nguyen, V.-H.; Mreńca-Kolasińska, A.; Watanabe, K.; Taniguchi, T.; Charlier, J.-C.; Stampfer, C.; Hackens, B. Optimizing Dirac fermions quasi-confinement by potential smoothness engineering. *2D Mater.* **2020**, *7*, 025037.

(37) Pioda, A.; Kičin, S.; Ihn, T.; Sigrist, M.; Fuhrer, A.; Ensslin, K.; Weichselbaum, A.; Ulloa, S. E.; Reinwald, M.; Wegscheider, W. Spatially Resolved Manipulation of Single Electrons in Quantum Dots Using a Scanned Probe. *Phys. Rev. Lett.* **2004**, *93*, 216801.

(38) Schnez, S.; Güttinger, J.; Huefner, M.; Stampfer, C.; Ensslin, K.; Ihn, T. Imaging localized states in graphene nanostructures. *Phys. Rev. B: Condens. Matter Mater. Phys.* **2010**, *82*, 165445.

(39) Walkup, D.; Ghahari, F.; Gutiérrez, C.; Watanabe, K.; Taniguchi, T.; Zhitenev, N. B.; Stroscio, J. A. Tuning single-electron charging and interactions between compressible Landau level islands in graphene. *Phys. Rev. B: Condens. Matter Mater. Phys.* **2020**, *101*, 035428.

(40) Bleszynski, A. C.; Zwanenburg, F. A.; Westervelt, R. M.; Roest, A. L.; Bakkers, E. P. A. M.; Kouwenhoven, L. P. Scanned Probe Imaging of Quantum Dots inside InAs Nanowires. *Nano Lett.* **2007**, *7*, 2559−2562.

(41) Liu, P.; Martins, F.; Hackens, B.; Desplanque, L.; Wallart, X.; Pala, M. G.; Huant, S.; Bayot, V.; Sellier, H. Formation of quantum dots in the potential fluctuations of InGaAs heterostructures probed by scanning gate microscopy. *Phys. Rev. B: Condens. Matter Mater. Phys.* **2015**, *91*, 075313.

(42) Rosenblum, S.; Lovsky, Y.; Arazi, L.; Vollmer, F.; Dayan, B. Cavity ring-up spectroscopy for ultrafast sensing with optical microresonators. *Nat. Commun.* **2015**, *6*, 6788.

https://doi.org/10.1021/acs.nanolett.1c03451
Nano Lett. 2022, 22, 128−134